










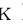



Flashlights: More than A Dozen High-Significance Microlensing Events of Extremely Magnified Stars in Galaxies at Redshifts $z = 0.7\text{--}1.5$

PATRICK L. KELLY ¹, WENLEI CHEN ¹, AMRUTH ALFRED,² THOMAS J. BROADHURST ³, JOSE M. DIEGO ⁴,
NAJMEH EMAMI,¹ ALEXEI V. FILIPPENKO ⁵, ALLISON KEEN,¹ SUNG KEI LI ², JEREMY LIM,² ASHISH K. MEENA ⁶,
MASAMUNE OGURI ⁷, CLAUDIA SCARLATA,¹ TOMMASO TREU ⁸, HAYLEY WILLIAMS,¹ LILIYA L.R. WILLIAMS ¹,
RUI ZHOU,¹ ADI ZITRIN ⁶, RYAN J. FOLEY,⁹ SAURABH W. JHA ¹⁰, NICK KAISER,¹¹ VIHANG MEHTA,¹ STEVEN RIECK,¹
LAURA SALO,¹ NATHAN SMITH ¹² AND DANIEL R. WEISZ⁵

¹Minnesota Institute for Astrophysics, University of Minnesota, 116 Church Street SE, Minneapolis, MN 55455, USA

²Department of Physics, The University of Hong Kong, Pokfulam Road, Hong Kong

³Ikerbasque Foundation, University of the Basque Country, DIPIC Donostia, Spain

⁴IFCA, Instituto de Física de Cantabria (UC-CSIC), Av. de Los Castros s/n, 39005 Santander, Spain

⁵Department of Astronomy, University of California, Berkeley, CA 94720-3411, USA

⁶Physics Department, Ben-Gurion University of the Negev, P.O. Box 653, Beer-Sheva 8410501, Israel

⁷Center for Frontier Science, Chiba University, 1-33 Yayoi-cho, Inage-ku, Chiba 263-8522, Japan; Department of Physics, Graduate School of Science, Chiba University, 1-33 Yayoi-Cho, Inage-Ku, Chiba 263-8522, Japan

⁸Department of Physics and Astronomy, University of California, Los Angeles, CA 90095

⁹Department of Astronomy and Astrophysics, UCO/Lick Observatory, University of California, 1156 High Street, Santa Cruz, CA 95064, USA

¹⁰Department of Physics and Astronomy, Rutgers, The State University of New Jersey, Piscataway, NJ 08854, USA

¹¹Laboratoire de Physique de l'Ecole Normale Supérieure, ENS, Université PSL, CNRS, Sorbonne Université, Université de Paris, Paris, France

¹²Department of Astronomy, University of Arizona, Tucson, AZ 85721, USA

ABSTRACT

Once only accessible in nearby galaxies, we can now study individual stars across much of the observable universe aided by galaxy-cluster gravitational lenses. When a star, compact object, or multiple such objects in the foreground galaxy-cluster lens become aligned, they can magnify a background individual star, and the timescale of a magnification peak can limit its size to tens of AU. The number and frequency of microlensing events therefore opens a window into the population of stars and compact objects, as well as high-redshift stars. To assemble the first statistical sample of stars in order to constrain the initial mass function (IMF) of massive stars at redshift $z = 0.7\text{--}1.5$, the abundance of primordial black holes in galaxy-cluster dark matter, and the IMF of the stars making up the intracluster light, we are carrying out a 192-orbit program with the *Hubble Space Telescope* called “Flashlights,” which is now only two-thirds complete owing to scheduling challenges. We use the ultrawide F200LP and F350LP long-pass WFC3 UVIS filters and conduct two 16-orbit visits separated by one year. Having an identical roll angle during both visits, while difficult to schedule, yields extremely clean subtraction. Here we report the discovery of more than a dozen bright microlensing events, including multiple examples in the famous “Dragon Arc” discovered in the 1980s, as well as the “Spocks” and “Warhol” arcs that have hosted already known supergiants. The ultradeep observer-frame ultraviolet-through-optical imaging is sensitive to hot stars, which will complement deep *James Webb Space Telescope* infrared imaging. We are also acquiring Large Binocular Telescope LUCI and Keck-I MOSFIRE near-infrared spectra of the highly magnified arcs to constrain their recent star-formation histories.

1. INTRODUCTION

Extreme gravitational lensing magnification (up to several thousand) of individual high-redshift stars by a foreground galaxy cluster, a newly discovered phenomenon (Kelly et al. 2018; Rodney et al. 2018; Chen et al. 2019; Kaurov et al. 2019; Welch et al. 2022; Diego

et al. 2022a; Chen et al. 2022; Diego et al. 2022b), has the ability to address three major outstanding questions. (a) What is dark matter? Despite decades of searches, the constituents of dark matter remain unidentified. (b) How was the universe reionized? The magnifying power of galaxy-cluster lenses holds great potential for studying faint, high-redshift galaxies, provided one can construct sufficiently accurate lens models (e.g., Bouwens et al. 2017). (c) How do stellar populations at redshift $z = 1-2$ differ from those in the nearby universe? We have only been able to study the composite spectral energy distributions (SEDs) of their luminous stars.

To address the major questions outlined above, we are carrying out ultradeep *Hubble Space Telescope* (*HST*) observations of the six Hubble Frontier Field (HFF; Lotz et al. 2017) clusters. These targets – Abell 2744, MACSJ0416.1-2403, MACSJ0717.5+3745, MACSJ1149.5+2223, Abell S1063, and Abell 370 – are among the most powerful gravitational lensing clusters and have multiband optical through infrared (IR) *HST* imaging observations as part of the 840-orbit HFF program. The HFF survey obtained optical imaging of each galaxy-cluster field in two-orbit visits spread across a period of approximately a month. For a single two-orbit visit using the ACS WFC F606W filter, the 5σ limiting AB (Oke & Gunn 1983) magnitude was 28.1 within a $0''.2$ -radius aperture (28.7 for an “optimal” extraction), according to the Exposure Time Calculator (ETC)¹. Considering a single week of HFF visits amounting to a total of six orbits, the limiting magnitude in the F606W filter, for example, was 28.7 (or 29.3 for an optimal measurement).

Since the expected timescale for a $\sim 10 R_{\odot}$ star to cross a caustic can be only hours (Miralda-Escude 1991), we aimed to carry out a two-epoch *HST* program of WFC3 UVIS observations (see Fig. 1) of galaxy clusters with a single-visit 5σ limiting magnitude of 30 (or optimal 31.1), ~ 2 mag deeper than each HFF visit, and ~ 1.3 mag deeper than each week of HFF visits. While the HFF obtained imaging from the optical through the near-infrared, our program includes observations with the ultraviolet-through-optical F200LP filter for sensitivity to emission from hot stars. The aim of the program is to find the first statistical samples of both microlensing events and pairs of magnified stellar images.

Close to a so-called fold caustic, the area in the source plane with magnification exceeding a value μ scales as μ^{-2} . By carrying out a survey with single-visit sensitivity ~ 1.3 mag (a factor of ~ 3 in flux) greater than

that of a single week of HFF imaging, we require magnifications that are an equal factor of 3 smaller for detection. Consequently, to first order, a factor of ~ 9 greater number of stars through their microlensing events can be expected. For microlensing events with durations of only hours, the ~ 2 mag difference in sensitivity corresponds to a factor of ~ 36 . The extremely deep imaging also enables several additional high-impact investigations, and is needed to interpret *James Webb Space Telescope* (*JWST*) observations of the HFFs.

In Section 2, we describe the principal science motivation for the Flashlights survey. Four of the six target HFF galaxy-cluster fields have now been visited twice, and Section 3 presents the high-significance microlensing events that we have detected. We discuss conclusions and implications from the current analysis of the data in Section 4.

2. SCIENCE DRIVERS

2.1. Dark Matter

Despite decades of searches, the constituents of $\sim 85\%$ of the matter in the universe remain unidentified. The newly discovered extreme magnification of high-redshift stars provides an entirely new and highly sensitive probe of the nature of dark matter. First, the potential of a galaxy cluster acts to exaggerate the Einstein radii of objects in its intracluster medium by factors of up to ~ 100 near its critical curves, dramatically enlarging microlensing ability (Diego et al. 2018; Venumadhav et al. 2017). Second, light traveling through a cluster (or a galaxy) near its critical curve traverses an extreme density of dark matter. Consequently, microlensing fluctuations of background stars should reveal even a small fraction (1–2%) of dark matter in the form of compact objects (Oguri et al. 2018).

Primordial black holes (PBHs) could have formed from perturbations in (for example) an inflaton or spectator field in the early universe. Currently, Galactic (Tisserand et al. 2007; Alcock et al. 2001) and quasar (Mediavilla et al. 2017) microlensing could allow PBHs with $10^{-3} M_{\odot} < M < 10^2 M_{\odot}$ to account for up to 3–10% of dark matter. Limits on their abundance place constraints on the primordial power spectrum associated with inflation (e.g., Carr et al. 2017).

The Laser Interferometer Gravitational-Wave Observatory (LIGO) is now able to detect the coalescence of neutron-star (Abbott et al. 2017) and black-hole (Abbott et al. 2016a,b) binary systems. LIGO and surveys of X-ray binary systems, however, are not sensitive to the populations of either *single* black holes or binary systems with wide separations.

¹ <https://etc.stsci.edu/etc/input/acs/imaging/>

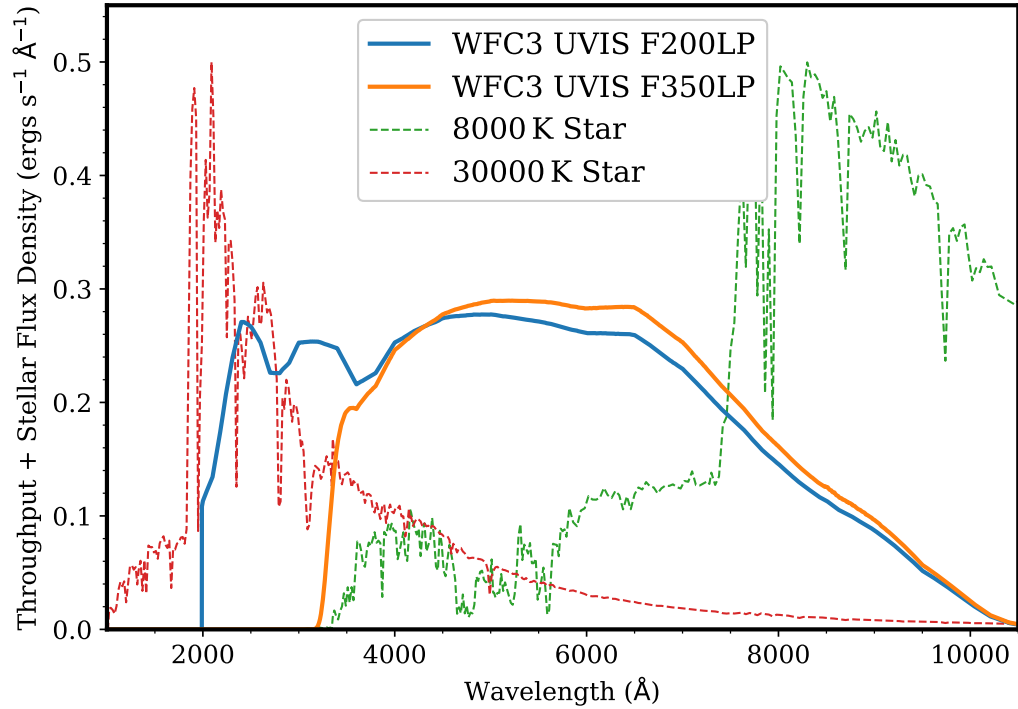


Figure 1. The survey will observe each of six HFF galaxy clusters at two epochs. During each 16-orbit visit, imaging alternates between orbits with integrations in WFC3 F200LP and WFC3 F350LP. The full throughputs of ACS WFC CLEAR and WFC3 F200LP as well as the SEDs of two stars at $z = 1$ are plotted here. The differences between the two filters provides constraints on the SED (including the reddening) of each star.

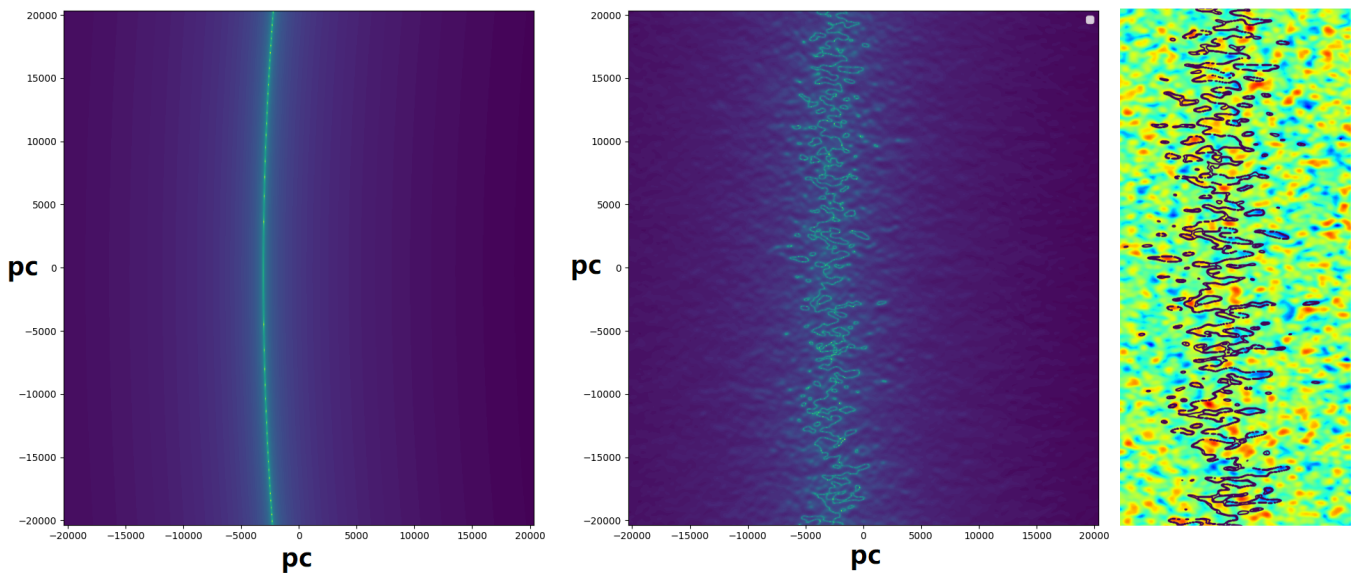


Figure 2. Effect of wave dark matter on gravitational lensing magnification adjacent to the galaxy cluster’s critical curve. *Left panel:* the magnification surrounding the critical curve of a galaxy cluster with mass similar to that of Abell 370 given a simply-parameterized smooth dark matter halo at the cluster scale and for individual cluster members. *Middle panel:* the magnification when the dark matter consists of ultralight bosons (ψ DM). *Right panel:* projected density fluctuations arising from ψ DM along with contours indicating regions of magnification of over 10^3 .

At low optical depths for microlensing, the frequency of microlensing events should increase in approximately

direct proportion to the mass density of microlenses.

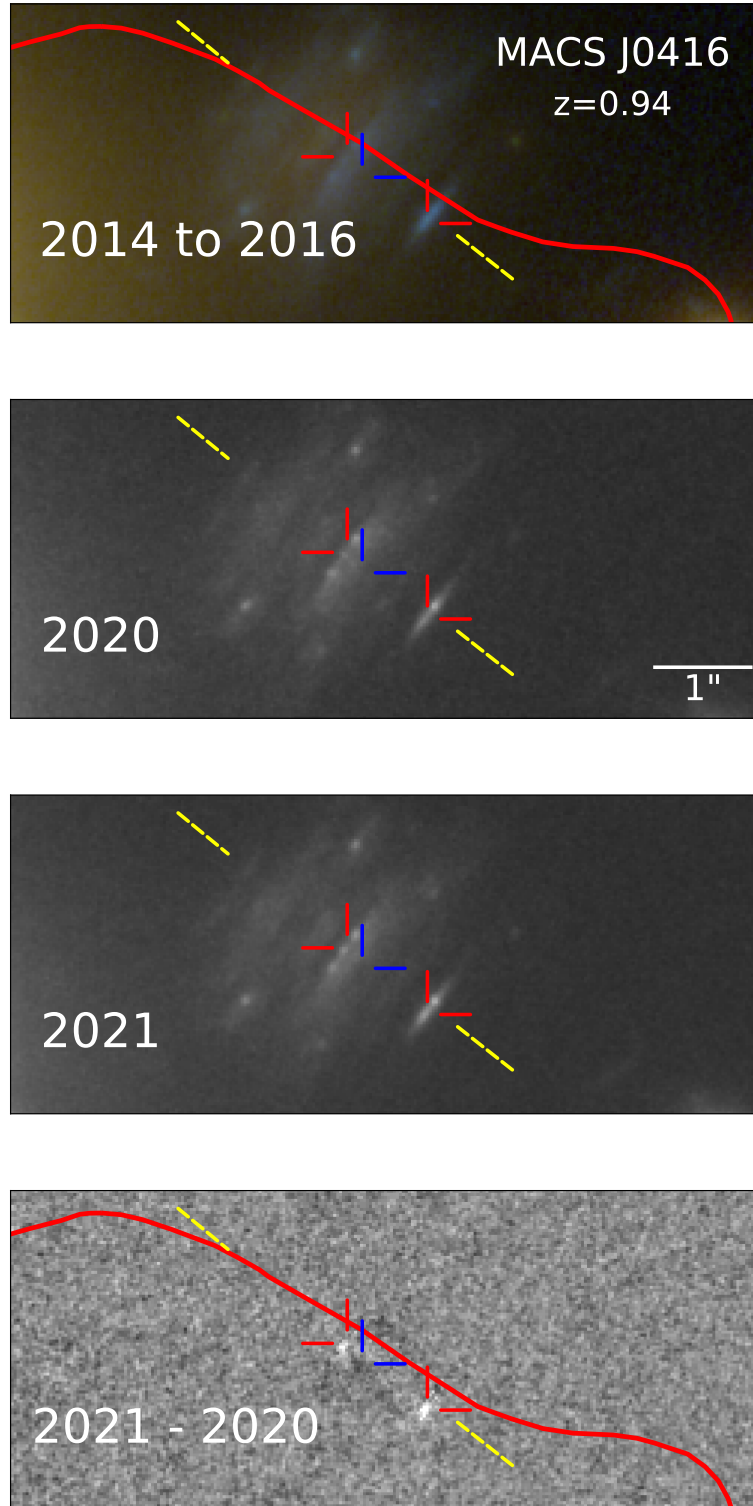


Figure 3. Microlensing events within $< 0''.1$ of the galaxy cluster critical curve in an arc at $z = 0.94$ in the MACS J0416 field. The upper panel shows a color-composite image from HFF imaging, the middle two panels show Flashlights F200LP imaging from 2020 and 2021, and the bottom panel indicates the difference of the two epochs. The peak visible in the bottom panel that is farthest to the right corresponds to one of the images of a highly magnified blue supergiant, “Warhol” (Chen et al. 2019; Kaurov et al. 2019). Red hatches correspond to peaks detected in the 2021 imaging, and blue hatches correspond to those present in the 2020 imaging. Yellow dashed lines mark approximately the line of symmetry of the arc, which corresponds closely to the critical curve. The red solid line marks the location of the galaxy cluster’s critical curve according to the simply-parameterized Keeton model (v4) available from the HFF website (Keeton 2010), although the model does not use the pairs of knots visible in the arc as constraints.

Moreover, the density of foreground intracluster stars along the line of sight toward giant arcs with $z = 0.7$ – 1.5 that straddle the critical curve are $\sim 1\%$ of the projected density of dark matter. Therefore, the number of microlensing events will provide a straightforward test of the abundance of PBHs comprising $\sim 1\%$ of dark matter across an extremely broad mass range of at least $10^{-5} < m/M_{\odot} < 100$.

When a strongly lensed star lies close to a fold caustic in the source plane, its two most highly magnified images will appear as a *pair* straddling the critical curve. When an object in the cluster becomes temporarily aligned with a background lensed star, one of these images brightens (or fades) temporarily as has been observed for both Icarus (Kelly et al. 2018) and Warhol (Chen et al. 2019; Kaurov et al. 2019). Dai et al. (2018) show that the presence of subhalos such as those expected in the Λ CDM paradigm should imprint detectable $0''.03$ – $0''.1$ deflections in the positions of pairs of lensed images of background stars, corresponding to halos of $\sim 10^7$ – $10^9 M_{\odot}$. Low-mass halos have been claimed to be identified in optical observations of galaxy-scale gravitational lenses (Vegetti et al. 2010, 2012) as well as at submillimeter wavelengths in the well-resolved Einstein ring galaxy SDP.81 (Hezaveh et al. 2016). A complementary statistical approach has found evidence for subhalos from analysis of flux anomalies (Nierenberg et al. 2014; Gilman et al. 2020). In principle, several magnified stars along a giant arc may be sufficient to detect the presence of such subhalos depending on the degree of tidal stripping.

In the context of “wave” dark matter (ψ DM), consisting of ultralight bosons, substructure is pervasive, caused by interference on the de Broglie scale within galaxy and cluster halos (Schive et al. 2014; Hui et al. 2017; Mocz et al. 2017). The de Broglie wavelength sets the scale of substructure fluctuations, ranging from several parsecs for clusters to ~ 1 kpc for dwarf galaxies for a boson mass of $\sim 10^{-22}$ eV (Pozo et al. 2021) as the de Broglie wavelength scales inversely with momentum. The effect of this density modulation for lensing is predicted to produce highly corrugated critical curves (Chan et al. 2020). As shown in Fig. 2, we can approximate the projected density field expected for a massive galaxy cluster using the same procedure for galaxies as described by Alfred et al. (2022, submitted). Notice in particular how small “islands” of high magnification are expected to be significantly offset from the location of a galaxy cluster’s critical curve, surrounding individual positive and negative density fluctuations that are depicted as red and blue (respectively). Consequently, individual stars may be highly magnified at projected

positions that are relatively far from the Einstein radius, providing a testable prediction of ψ DM.

2.2. Improving Galaxy Clusters as Tools

Near the critical curves of galaxy clusters, *JWST* should be sensitive to sources as faint as ~ 35 AB mag, making it possible in principle to measure the properties of the low-luminosity galaxies thought to drive reionization. In areas of high magnification, it is crucial to obtain sufficient information to constrain the lens models well enough to determine accurate luminosities and volumes. Achieving this goal requires deep high-resolution images to identify dozens of multiply-imaged systems, as well as spectroscopic confirmations of large numbers of them.

In the image plane on the sky, magnification falls steeply as the inverse of the distance from the critical curve. In regions that currently lack sufficient constraints, however, lens models can disagree about the location of the critical curve by of order an arcsecond, which is a principal factor that explains the uncertain magnification of some high-redshift objects. As Icarus and Warhol demonstrate, each of the expected pairs of highly magnified stellar images (and those of star clusters) will *pinpoint* the location of the critical curve. Furthermore, the probability of a microlensing event with a given peak magnification should drop approximately as the inverse of the offset from the critical curve to the fourth power (Kelly et al. 2018). Therefore, the microlensing events will also trace critical curves, albeit not as exactly.

2.3. Stellar Populations in Galaxies at $z = 1$ – 2

Galaxies near cosmic noon (at $z = 1$ – 2) are more intensely star forming and exhibit more extreme nebular emission-line ratios than nearby galaxies (e.g., Steidel et al. 2014; Sanders et al. 2015). In nearby galaxies, we can resolve individual massive stars, and thereby constrain their luminosity functions and the upper end of the initial mass function (IMF). Currently, however, we are only able to study the composite SEDs of $z = 1$ – 2 stellar populations, which limits our ability to constrain the upper end of the IMF. Improved constraints are necessary, because luminous stars are responsible for driving the evolution of galaxies through their ionizing flux, winds, and energy input from supernovae. Moreover, the IMF is a key parameter that affects interpretation of the observed properties of galaxy populations at high redshift (e.g., Narayanan & Davé 2012).

The number of detections of microlensing events should depend on the stellar luminosity function (see Extended Data Fig. 5 of Kelly et al. 2018), and there-

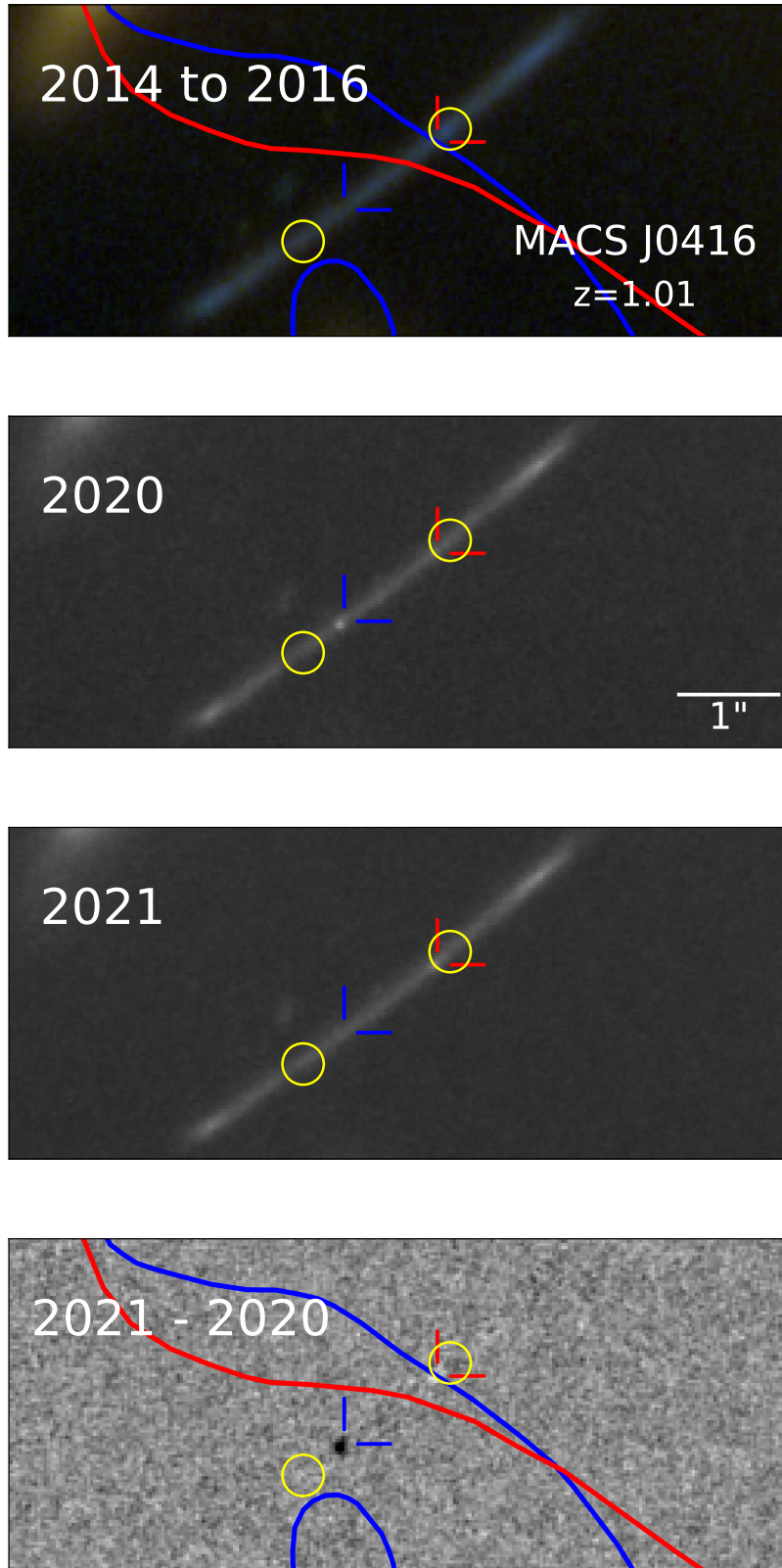


Figure 4. Microlensing events in the “Spocks” arc at $z = 1.00$ in the MACSJ0416 galaxy-cluster field. We overplot the critical curve from the Zitrin Light-Traces-Mass model (v1) (Zitrin et al. 2013) in red, and the Sharon (Johnson et al. 2014) simply-parameterized model (v4cor) in blue. The locations of the two transients reported by Rodney et al. (2018) in HFF imaging acquired in 2014 are shown with yellow circles. The positions of the two high-significance events detected in Flashlights imaging are at distinct positions, and may correspond to counterimages of the Rodney et al. (2018) events.

fore the IMF. Consequently, the microlensing events detected by Flashlights will make it possible to measure the stellar luminosity function and upper end of the IMF across star-forming $z = 1\text{--}2$ galaxies that cross the critical curve.

The survey includes two visits to each cluster consisting of 16 contiguous orbits (or as close as possible), alternating between orbits with WFC3 UVIS F350LP and WFC3 UVIS F200LP integrations. Our initial strategy was to use ACS WFC CLEAR instead of WFC3 UVIS F350LP, but the point-spread function (PSF) was degraded in our first observations, of Abell 370. The two visits to each HFF cluster are separated by one year, so that we can take parallel field observations at the same roll angle which will serve as a control experiment.

A microlensing peak should have a duration R/v , where R is the size of the lensed source and v is the transverse velocity of the lensing system (Miralda-Escude 1991). Given the $\sim 1000\text{ km s}^{-1}$ expected transverse velocity of the cluster lens system, the several-week timescale of Icarus’ May 2016 microlensing peak (Kelly et al. 2018) implies that the source only extends for at most several tens of AU.

2.4. Enabling *JWST* Searches for Dropout Galaxies

A key objective of *JWST* is to answer the question of how the universe became reionized at $z > 6$ (e.g., Castellano et al. 2016). One main observable required to study the history of reionization is the rest-frame UV galaxy luminosity function, which constrains the total star-formation rate (SFR) at any given redshift. The principal technique for measuring the luminosity functions of high-redshift galaxies is to identify Lyman-break “dropout” galaxies. The ionizing continuum (below 912 \AA) of galaxies is strongly absorbed by neutral H I gas in the interstellar medium and in the surrounding circumgalactic and intergalactic medium. Additionally, the continuum between 912 and 1216 \AA is attenuated by the Ly α forest, created in discrete systems along the line of sight (Giavalisco 2002).

Typical Lyman-break colors (i.e., color difference between wavelengths redder and bluer than Ly α) used to select $z > 6$ galaxies amount to $\gtrsim 1$ mag (e.g., Finkelstein 2016, for a review). The Lyman break, however, can be mimicked by low-redshift faint galaxies showing intrinsically red colors, including from a strong Balmer break, across the filters used to perform the selection. These red low-redshift interlopers include $z \approx 2$ passive galaxies, dusty star-forming objects, or strong emission-line starbursting dwarfs (e.g., Livermore et al. 2018, Atek et al. 2011). A classic example is the putative $z \approx 11$ object identified by Laporte et al. (2011) as a

J -band dropout. In follow-up work, Hayes et al. (2012) demonstrated spectroscopically that the object in fact has $z \approx 2.1$, either a young heavily reddened starburst or a maximally old system with a very pronounced 4000 \AA break. Had $AB \approx 30$ optical imaging (blueward of the Lyman break) been available, this low-redshift contaminant could have been identified (Hayes et al. 2012).

Reaching AB magnitudes of 30, the observations provide six benchmark fields for high-redshift galaxy searches with *JWST*. Specifically, the data will be unique to identify the population of $z \approx 2$ galaxies with colors mimicking those of $z = 7\text{--}12$ candidates.

3. HIGH-SIGNIFICANCE MICROLENSING EVENTS

In Table 1, we list high-significance detections of transients in a set of giant arcs in the Flashlights targets Abell 370, MACSJ0416, and Abell S1063 with repeat observations acquired as part of the Flashlights survey. There, we describe whether the transients are found adjacent ($\lesssim 0''.2$) to the critical curve of the galaxy cluster, and therefore are very likely to be microlensing events in regions of high magnification exceeding ~ 100 . A star adjacent to (and on the correct side of) a fold caustic in the source plane will appear as a pair of highly magnified images. The relative time delay between such a pair of highly magnified images is only of order days. Given the typical timescales of outbursts of weeks to months of massive stars, any strong asymmetry between the fluxes of a pair of images can only be explained by stellar microlensing. Many of the microlensing events appear in pairs across the critical curve, and simulations by Kelly et al. (2018) show that the same star is often responsible for microlensing events on both sides of the critical curve.

Fig. 3 shows the prominent arc at $z = 0.94$ in the MACSJ0416 galaxy-cluster field where the “Warhol” (Chen et al. 2019; Kaurov et al. 2019) event was discovered. The clear fold symmetry of the Warhol arc at $z = 0.94$ makes it possible to identify the location of the critical curve which corresponds to the line of symmetry, and we detect three microlensing events in the arc. The middle two panels show 2020 and 2021 F200LP Flashlights imaging, respectively, while the bottom panel shows a difference image made by subtracting the imaging acquired in 2021 from that taken in 2020. The red and blue cross hatches indicate the locations of the high-significance transients. We overplot, as an example of a simply parameterized prediction, the critical curves for Light-Traces-Mass (v1) Zitrin et al. (2013) and the simply parameterized Sharon (v4cor) Johnson

| Cluster | RA (deg.) | Dec (deg.) | z | F200LP Signif. | F350LP Signif. | μ GLAFIC* | μ Gravlens* | Approx. CC Proximity |
|-------------|--------------|---------------|-------------------|-------------------|-------------------|------------------|--------------------|-------------------------|
| Abell 370 | 39.9704121 | -1.5848997 | 0.73 ^a | 19.0 | ... | 1700 | 5800 | $\lesssim 0.1''$ |
| Abell 370 | 39.9718583 | -1.5848133 | 0.73 ^a | 5.2 | ... | 60 | 26 | $\lesssim 0.3''$ |
| Abell 370 | 39.9711217 | -1.5848492 | 0.73 ^a | 3.3 | ... | 30 | 28 | $\lesssim 0.3''$ |
| Abell 370 | 39.9702708 | -1.5848842 | 0.73 ^a | 4.7 | ... | 170 | 89 | $\lesssim 0.1''$ |
| Abell 370 | 39.9719888 | -1.5848139 | 0.73 ^a | 4.5 | ... | 50 | 15 | $\lesssim 0.3''$ |
| Abell 370 | 39.9710843 | -1.5848642 | 0.73 ^a | 5.1 | ... | 25 | 20 | $\lesssim 0.3''$ |
| Abell 370 | 39.9691621 | -1.5846231 | 0.73 ^a | 5.3 | ... | 15 | 10 | $\lesssim 0.1''$ |
| Abell 370 | 39.9672042 | -1.5849367 | 1.26 ^b | 5.9 | ... | 44 | 60 | $\sim 0.6''$ |
| Abell S1063 | 342.1925167 | -44.5304881 | 1.26 ^c | 5.8 | 3.3 | 110 | 100 | $\lesssim 0.1''$ |
| Abell S1063 | 342.1924193 | -44.5304881 | 1.26 ^c | 31.0 | 16.3 | 190 | 180 | $\lesssim 0.3''$ |
| Abell S1063 | 342.1924847 | -44.5304337 | 1.26 ^c | 7.1 | 3.5 | 250 | 210 | $\lesssim 0.2''$ |
| Abell S1063 | 342.1894900 | -44.5290447 | 0.73 ^d | 7.2 | 4.9 | 28 | 32 | $\lesssim 1''$ |
| Abell S1063 | 342.1890363 | -44.5286928 | 0.73 ^d | 8.2 | 0.0 | 20 | 27 | $\lesssim 3''$ |
| Abell S1063 | 342.1952641 | -44.5279212 | 1.23 ^e | 10.4 | 8.0 | 550 | 450 | $\lesssim 0.1''$ |
| MACS J0416 | 64.0388904 | -24.0701557 | 1.01 ^f | 18.7 | 12.7 | 55 | 77 | $\lesssim 0.2''$ |
| MACS J0416 | 64.0386110 | -24.0699715 | 1.01 ^f | 18.7 | 12.7 | 78 | 1200 | $\lesssim 0.2''$ |
| MACS J0416 | 64.0363046 | -24.0675050 | 0.94 ^g | 10.2 | 8.3 | 25 | 60 | $\lesssim 0.1''$ |
| MACS J0416 | 64.0365524 | -24.0673339 | 0.94 ^g | 5.9 | 6.7 | 30 | 70 | $\lesssim 0.1''$ |
| MACS J0416 | 64.0364386 | -24.0674422 | 0.94 ^g | 2.7 | 4.5 | 21 | 50 | $\lesssim 0.1''$ |
| MACS J0416 | 64.0365133 | -24.0673656 | 0.94 ^g | 2.6 | 2.6 | 29 | 60 | $\lesssim 0.1''$ |

Table 1. Examples of high-significance transients in strongly lensing arcs. (a) Soucail et al. (1988); (b) Lagattuta et al. (2017); (c) Caminha et al. (2016); (d) Diego et al. (2016); (e) Karman et al. (2017); (f) Rodney et al. (2018); (g) Caminha et al. (2017).

et al. (2014) models available on the HFF website². The microlensing events include detection of variability at location of the pair of images of the “Warhol” blue supergiant.

In Fig. 4, we also plot our detection of two transients in the arc in the MACS J0416 field of the “Spocks” ($z = 1.01$) (Rodney et al. 2018) events. The locations of the two new events identified by Flashlights differ from those of the Spocks events whose positions we identify.

Fig. 5 shows high-significance microlensing events that we detect in Flashlights imaging close to the critical curve of a giant arc in the Abell S1063 galaxy-cluster field at $z = 1.26$. In the case of this arc, the location of the galaxy cluster’s critical curve is constrained by the mirrored positions of knots. Finally, we detect two high-significance transients in an adjacent arc in this field with a lower redshift of 0.73. Fig. 6 plots the locations of these transients in F200LP imaging, and the critical curve we show is that from the Williams free-form GRALE (Ghosh et al. 2021) HFF model (v4.1).

The upper panel of Fig. 7 shows a color-composite image of the “Dragon” arc at $z = 0.73$ (Soucail et al.

1988) constructed from HFF optical and near-IR imaging taken in 2014–2016. Superimposed are the critical curves of the WSLAP+ model (v4.1) (Diego et al. 2005, 2007, 2016) and the GLAFIC model (v4) (Kawamata et al. 2018, 2016; Oguri 2010). Three of the transients in the Dragon arc are very likely to be microlensing events, given their close proximity to the critical curve of the galaxy cluster. The four additional transients, which appear in pairs, may also be microlensing events if they are located sufficiently close to the critical curves of nearby cluster members. Finally, in Meena et al. (2022), we present an analysis of a transient in an additional arc at $z = 1.26$ in the Abell 370 galaxy-cluster field that we infer to likely be a microlensing event, despite a relatively large offset from the critical curve.

4. CONCLUSIONS

We show that sufficiently deep exposures reveal many microlensing events in individual galaxies at $z = 0.7$ – 1.5 . We anticipate that deep, repeat visits with *JWST* will reveal populations of highly magnified stars. Given its powerful near-IR sensitivity, *JWST* will detect much cooler stars, including luminous red supergiants. At the same time, once completed, Flashlights will provide a

² <https://archive.stsci.edu/prepds/frontier/lensmodels/>

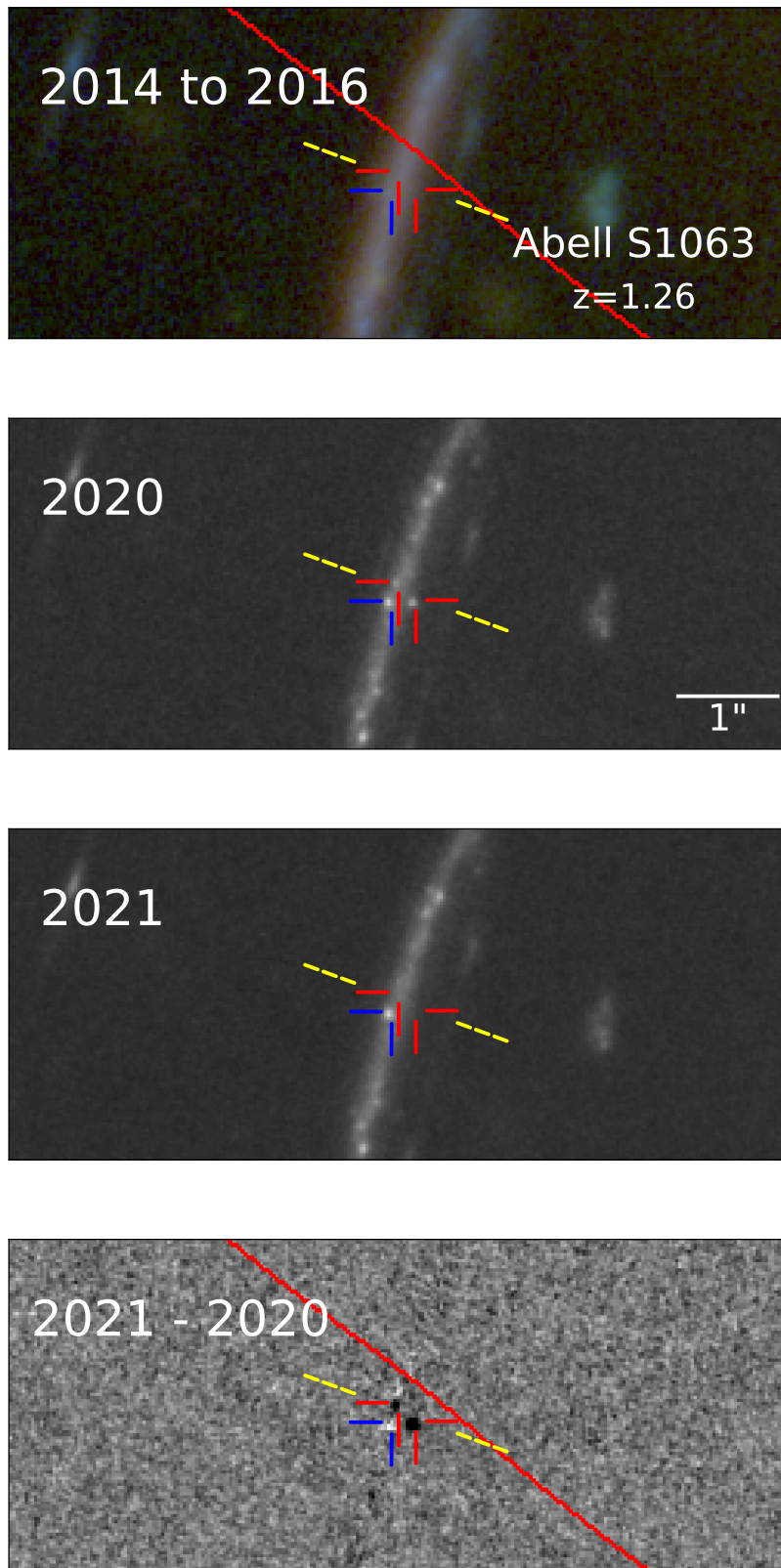


Figure 5. Three high-significance microlensing events in a giant arc at $z = 1.26$ in the Abell S1063 galaxy cluster field. Yellow dashed lines mark approximately the line of symmetry of the arc, which corresponds closely to the critical curve. The plotted critical curve is that from the Keeton HFF simply-parameterized model (v4) (Keeton 2010).

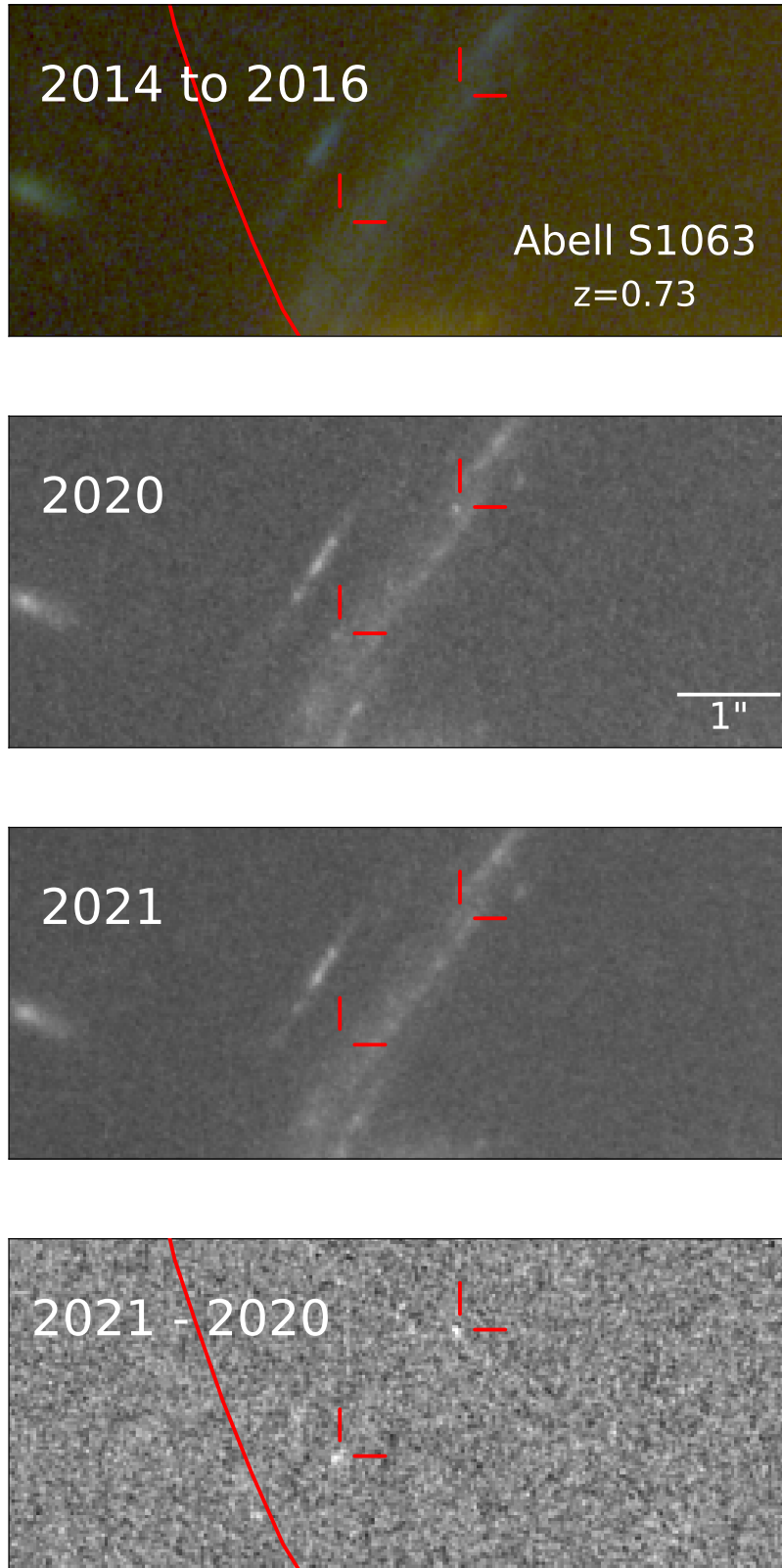


Figure 6. Two high-significance candidate microlensing events in a giant arc at $z = 0.73$ in the Abell S1063 galaxy cluster field. The plotted critical curve is that from the Williams free-form **GraLe** (Ghosh et al. 2021) HFF model (v4.1).

complementary dataset with sensitivity to the population of hot stars near the peak of cosmic star formation.

Through detections of the first substantial sample of highly magnified stars, Flashlights will enable a novel

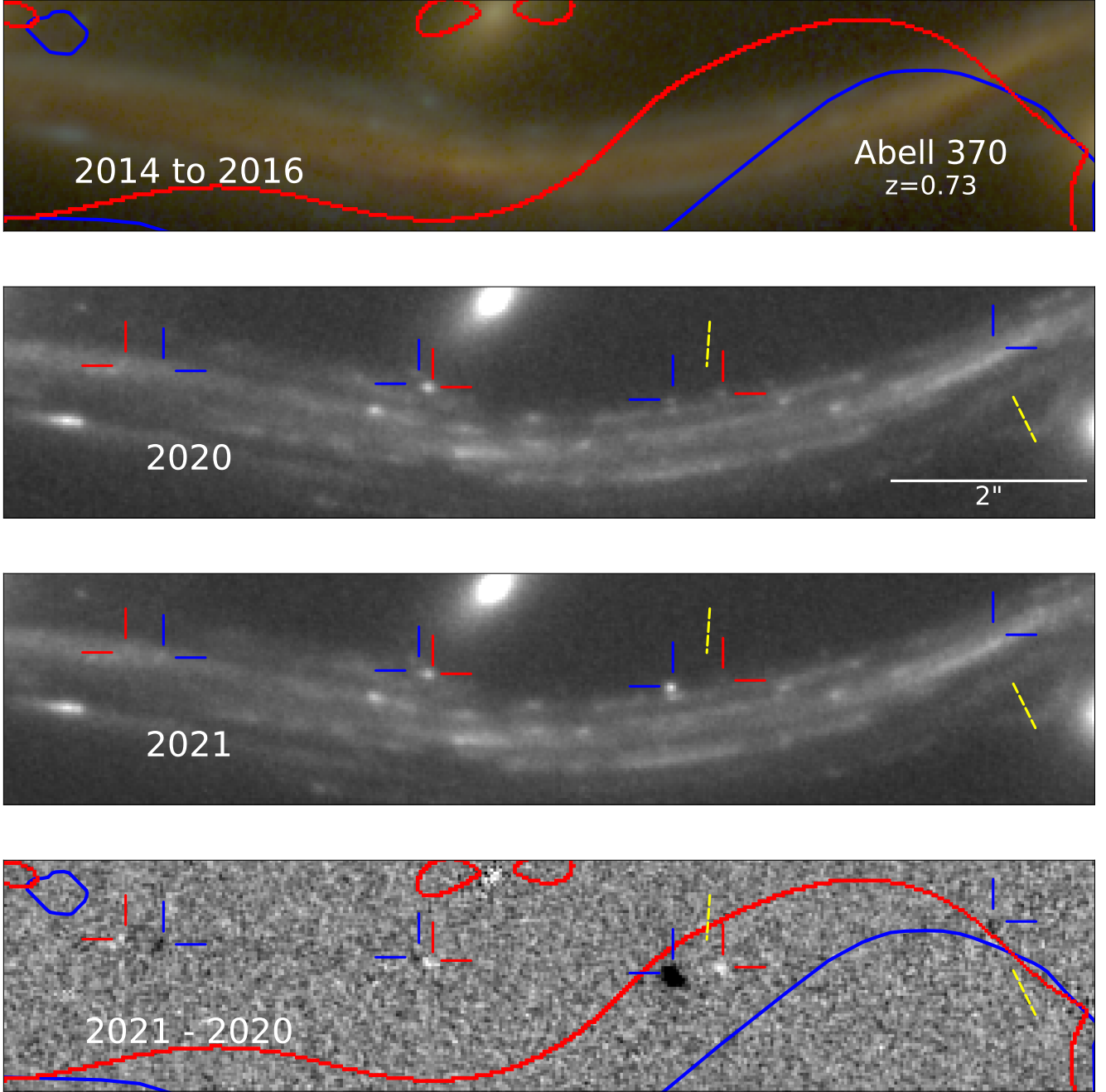


Figure 7. High-significance microlensing events adjacent to a model critical curve in the famous “Dragon” giant arc at $z = 0.725$ (Soucail et al. 1988). The critical curve for the WSLAP+ model (v4.1) (Diego et al. 2005, 2007, 2016) is shown in blue, and that for the simply-parameterized GLAFIC (Kawamata et al. 2018, 2016; Oguri 2010) code (v4) is in red. The locations of the smaller critical curves associated with cluster members are not yet well constrained.

probe of the nature of dark matter as well as the IMF of luminous stars at $z = 0.7\text{--}1.5$. The positions of stars provide a new constraint on galaxy-cluster models through accurate measurements of the location of the cluster critical curve. Finally, the extremely deep UV through optical wideband imaging provides a power-

ful means to identify low-redshift interlopers in Lyman-break dropout samples.

We thank Patricia Royale at the Space Telescope Science Institute (STScI) for her terrific effort scheduling the program, and our instrument scientist Annalisa Calamida for her careful review of the program. This re-

search was supported by NASA/*HST* grants GO-15936 and GO-16278 from STScI, which is operated by the Association of Universities for Research in Astronomy, Inc., under NASA contract NAS5-26555, and also by grant JPL-1659411 to support ground-based follow-up observations with the Keck-I telescope. A.V.F. is grateful for additional financial support from the Christopher R. Redlich Fund and numerous individual donors. P.L.K. acknowledges support through NSF grant AST-1908823, and NASA Keck JPL grant 1659411. This work was supported by JSPS KAKENHI grants JP22H01260, JP20H05856, and JP20H00181. Work by S.K.L. and J.L. is supported by the Collaborative Research Fund under grant C6017-20G, which is issued by the Research Grants Council of Hong Kong S.A.R. A.K.M. and A.Z. acknowledge support by grant 2020750 from the United States-Israel Binational Science Foundation (BSF) and grant 2109066 from the United States National Science

Foundation (NSF), and by the Ministry of Science & Technology, Israel.

Some of the data presented herein were obtained at the W. M. Keck Observatory, which is operated as a scientific partnership among the California Institute of Technology, the University of California, and NASA; the observatory was made possible by the generous financial support of the W. M. Keck Foundation. We acknowledge the HFF Lens Model website that is hosted by the Mikulski Archive for Space Telescopes (MAST) at STScI.

Facilities: HST (WFC3); Large Binocular Telescope (LUCI); Keck (MOSFIRE)

Software: Drizzlepac (Gonzaga 2012); Source Extractor (Bertin & Arnouts 1996)

REFERENCES

- Abbott, B. P., Abbott, R., Abbott, T. D., et al. 2016a, *Physical Review Letters*, 116, 061102, doi: [10.1103/PhysRevLett.116.061102](https://doi.org/10.1103/PhysRevLett.116.061102)
- . 2016b, *Physical Review Letters*, 116, 241103, doi: [10.1103/PhysRevLett.116.241103](https://doi.org/10.1103/PhysRevLett.116.241103)
- . 2017, *Physical Review Letters*, 119, 161101, doi: [10.1103/PhysRevLett.119.161101](https://doi.org/10.1103/PhysRevLett.119.161101)
- Alcock, C., Allsman, R. A., Alves, D. R., et al. 2001, *ApJL*, 550, L169, doi: [10.1086/319636](https://doi.org/10.1086/319636)
- Atek, H., Siana, B., Scarlata, C., et al. 2011, *ApJ*, 743, 121, doi: [10.1088/0004-637X/743/2/121](https://doi.org/10.1088/0004-637X/743/2/121)
- Bertin, E., & Arnouts, S. 1996, *AJ*, 117, 393
- Bouwens, R. J., Oesch, P. A., Illingworth, G. D., Ellis, R. S., & Stefanon, M. 2017, *ApJ*, 843, 129, doi: [10.3847/1538-4357/aa70a4](https://doi.org/10.3847/1538-4357/aa70a4)
- Caminha, G. B., Grillo, C., Rosati, P., et al. 2016, *A&A*, 587, A80, doi: [10.1051/0004-6361/201527670](https://doi.org/10.1051/0004-6361/201527670)
- . 2017, *A&A*, 600, A90, doi: [10.1051/0004-6361/201629297](https://doi.org/10.1051/0004-6361/201629297)
- Carr, B., Tenkanen, T., & Vaskonen, V. 2017, *PhRvD*, 96, 063507, doi: [10.1103/PhysRevD.96.063507](https://doi.org/10.1103/PhysRevD.96.063507)
- Castellano, M., Amorín, R., Merlin, E., et al. 2016, *A&A*, 590, A31, doi: [10.1051/0004-6361/201527514](https://doi.org/10.1051/0004-6361/201527514)
- Chan, J. H. H., Schive, H.-Y., Wong, S.-K., Chiueh, T., & Broadhurst, T. 2020, *PhRvL*, 125, 111102, doi: [10.1103/PhysRevLett.125.111102](https://doi.org/10.1103/PhysRevLett.125.111102)
- Chen, W., Kelly, P. L., Diego, J. M., et al. 2019, *ApJ*, 881, 8, doi: [10.3847/1538-4357/ab297d](https://doi.org/10.3847/1538-4357/ab297d)
- Chen, W., Kelly, P. L., Treu, T., et al. 2022, arXiv e-prints, arXiv:2207.11658. <https://arxiv.org/abs/2207.11658>
- Dai, L., Venumadhav, T., Kaurov, A. A., & Miralda-Escudé, J. 2018, ArXiv e-prints. <https://arxiv.org/abs/1804.03149>
- Diego, J. M., Broadhurst, T., Wong, J., et al. 2016, *MNRAS*, 459, 3447, doi: [10.1093/mnras/stw865](https://doi.org/10.1093/mnras/stw865)
- Diego, J. M., Pascale, M., Kavanagh, B. J., et al. 2022a, *A&A*, 665, A134, doi: [10.1051/0004-6361/202243605](https://doi.org/10.1051/0004-6361/202243605)
- Diego, J. M., Protopapas, P., Sandvik, H. B., & Tegmark, M. 2005, *MNRAS*, 360, 477, doi: [10.1111/j.1365-2966.2005.09021.x](https://doi.org/10.1111/j.1365-2966.2005.09021.x)
- Diego, J. M., Tegmark, M., Protopapas, P., & Sandvik, H. B. 2007, *MNRAS*, 375, 958, doi: [10.1111/j.1365-2966.2007.11380.x](https://doi.org/10.1111/j.1365-2966.2007.11380.x)
- Diego, J. M., Kaiser, N., Broadhurst, T., et al. 2018, *ApJ*, 857, 25, doi: [10.3847/1538-4357/aab617](https://doi.org/10.3847/1538-4357/aab617)
- Diego, J. M., Meena, A. K., Adams, N. J., et al. 2022b, arXiv e-prints, arXiv:2210.06514. <https://arxiv.org/abs/2210.06514>
- Finkelstein, S. L. 2016, *PASA*, 33, e037, doi: [10.1017/pasa.2016.26](https://doi.org/10.1017/pasa.2016.26)
- Ghosh, A., Williams, L. L. R., Liesenborgs, J., et al. 2021, *MNRAS*, 506, 6144, doi: [10.1093/mnras/stab1196](https://doi.org/10.1093/mnras/stab1196)
- Giavalisco, M. 2002, *ARA&A*, 40, 579, doi: [10.1146/annurev.astro.40.121301.111837](https://doi.org/10.1146/annurev.astro.40.121301.111837)
- Gilman, D., Birrer, S., Nierenberg, A., et al. 2020, *MNRAS*, 491, 6077, doi: [10.1093/mnras/stz3480](https://doi.org/10.1093/mnras/stz3480)
- Gonzaga, S. e. 2012, *The DrizzlePac Handbook*
- Hayes, M., Laporte, N., Pelló, R., Schaerer, D., & Le Borgne, J.-F. 2012, *MNRAS*, 425, L19, doi: [10.1111/j.1745-3933.2012.01293.x](https://doi.org/10.1111/j.1745-3933.2012.01293.x)

- Hezaveh, Y. D., Dalal, N., Marrone, D. P., et al. 2016, *ApJ*, 823, 37, doi: [10.3847/0004-637X/823/1/37](https://doi.org/10.3847/0004-637X/823/1/37)
- Hui, L., Ostriker, J. P., Tremaine, S., & Witten, E. 2017, *PhRvD*, 95, 043541, doi: [10.1103/PhysRevD.95.043541](https://doi.org/10.1103/PhysRevD.95.043541)
- Johnson, T. L., Sharon, K., Bayliss, M. B., et al. 2014, *ApJ*, 797, 48, doi: [10.1088/0004-637X/797/1/48](https://doi.org/10.1088/0004-637X/797/1/48)
- Karman, W., Caputi, K. I., Caminha, G. B., et al. 2017, *A&A*, 599, A28, doi: [10.1051/0004-6361/201629055](https://doi.org/10.1051/0004-6361/201629055)
- Kaurov, A. A., Dai, L., Venumadhav, T., Miralda-Escudé, J., & Frye, B. 2019, *ApJ*, 880, 58, doi: [10.3847/1538-4357/ab2888](https://doi.org/10.3847/1538-4357/ab2888)
- Kawamata, R., Ishigaki, M., Shimasaku, K., et al. 2018, *ApJ*, 855, 4, doi: [10.3847/1538-4357/aaa6cf](https://doi.org/10.3847/1538-4357/aaa6cf)
- Kawamata, R., Oguri, M., Ishigaki, M., Shimasaku, K., & Ouchi, M. 2016, *ApJ*, 819, 114, doi: [10.3847/0004-637X/819/2/114](https://doi.org/10.3847/0004-637X/819/2/114)
- Keeton, C. R. 2010, *Gen. Rel. Grav.*, 42, 2151, doi: [10.1007/s10714-010-1041-1](https://doi.org/10.1007/s10714-010-1041-1)
- Kelly, P. L., Diego, J. M., Rodney, S., et al. 2018, *Nature Astronomy*, 2, 334, doi: [10.1038/s41550-018-0430-3](https://doi.org/10.1038/s41550-018-0430-3)
- Lagattuta, D. J., Richard, J., Clément, B., et al. 2017, *MNRAS*, 469, 3946, doi: [10.1093/mnras/stx1079](https://doi.org/10.1093/mnras/stx1079)
- Laporte, N., Pelló, R., Schaerer, D., et al. 2011, *A&A*, 531, A74, doi: [10.1051/0004-6361/201015842](https://doi.org/10.1051/0004-6361/201015842)
- Livermore, R. C., Trenti, M., Bradley, L. D., et al. 2018, *ApJL*, 861, L17, doi: [10.3847/2041-8213/aacd16](https://doi.org/10.3847/2041-8213/aacd16)
- Lotz, J. M., Koekemoer, A., Coe, D., et al. 2017, *ApJ*, 837, 97, doi: [10.3847/1538-4357/837/1/97](https://doi.org/10.3847/1538-4357/837/1/97)
- Mediavilla, E., Jiménez-Vicente, J., Muñoz, J. A., Vives-Arias, H., & Calderón-Infante, J. 2017, *ApJL*, 836, L18, doi: [10.3847/2041-8213/aa5dab](https://doi.org/10.3847/2041-8213/aa5dab)
- Meena, A. K., Chen, W., Zitrin, A., et al. 2022, *arXiv e-prints*, arXiv:2211.01402. <https://arxiv.org/abs/2211.01402>
- Miralda-Escudé, J. 1991, *ApJ*, 379, 94, doi: [10.1086/170486](https://doi.org/10.1086/170486)
- Mocz, P., Vogelsberger, M., Robles, V. H., et al. 2017, *MNRAS*, 471, 4559, doi: [10.1093/mnras/stx1887](https://doi.org/10.1093/mnras/stx1887)
- Narayanan, D., & Davé, R. 2012, *MNRAS*, 423, 3601, doi: [10.1111/j.1365-2966.2012.21159.x](https://doi.org/10.1111/j.1365-2966.2012.21159.x)
- Nierenberg, A. M., Treu, T., Wright, S. A., Fassnacht, C. D., & Auger, M. W. 2014, *MNRAS*, 442, 2434, doi: [10.1093/mnras/stu862](https://doi.org/10.1093/mnras/stu862)
- Oguri, M. 2010, *PASJ*, 62, 1017, doi: [10.1093/pasj/62.4.1017](https://doi.org/10.1093/pasj/62.4.1017)
- Oguri, M., Diego, J. M., Kaiser, N., Kelly, P. L., & Broadhurst, T. 2018, *PhRvD*, 97, 023518, doi: [10.1103/PhysRevD.97.023518](https://doi.org/10.1103/PhysRevD.97.023518)
- Oke, J. B., & Gunn, J. E. 1983, *ApJ*, 266, 713, doi: [10.1086/160817](https://doi.org/10.1086/160817)
- Pozo, A., Broadhurst, T., de Martino, I., et al. 2021, *MNRAS*, 504, 2868, doi: [10.1093/mnras/stab855](https://doi.org/10.1093/mnras/stab855)
- Rodney, S. A., Balestra, I., Bradac, M., et al. 2018, *Nature Astronomy*, 2, 324, doi: [10.1038/s41550-018-0405-4](https://doi.org/10.1038/s41550-018-0405-4)
- Sanders, R. L., Shapley, A. E., Kriek, M., et al. 2015, *ArXiv e-prints*. <https://arxiv.org/abs/1509.03636>
- Schive, H.-Y., Chiueh, T., & Broadhurst, T. 2014, *Nature Physics*, 10, 496, doi: [10.1038/nphys2996](https://doi.org/10.1038/nphys2996)
- Soucail, G., Mellier, Y., Fort, B., Mathez, G., & Cailloux, M. 1988, *A&A*, 191, L19
- Steidel, C. C., Rudie, G. C., Strom, A. L., et al. 2014, *ApJ*, 795, 165, doi: [10.1088/0004-637X/795/2/165](https://doi.org/10.1088/0004-637X/795/2/165)
- Tisserand, P., Le Guillou, L., Afonso, C., et al. 2007, *A&A*, 469, 387, doi: [10.1051/0004-6361:20066017](https://doi.org/10.1051/0004-6361:20066017)
- Vegetti, S., Koopmans, L. V. E., Bolton, A., Treu, T., & Gavazzi, R. 2010, *MNRAS*, 408, 1969, doi: [10.1111/j.1365-2966.2010.16865.x](https://doi.org/10.1111/j.1365-2966.2010.16865.x)
- Vegetti, S., Lagattuta, D. J., McKean, J. P., et al. 2012, *Nature*, 481, 341, doi: [10.1038/nature10669](https://doi.org/10.1038/nature10669)
- Venumadhav, T., Dai, L., & Miralda-Escudé, J. 2017, *ApJ*, 850, 49, doi: [10.3847/1538-4357/aa9575](https://doi.org/10.3847/1538-4357/aa9575)
- Welch, B., Coe, D., Diego, J. M., et al. 2022, *Nature*, 603, 815, doi: [10.1038/s41586-022-04449-y](https://doi.org/10.1038/s41586-022-04449-y)
- Zitrin, A., Meneghetti, M., Umetsu, K., et al. 2013, *ApJL*, 762, L30, doi: [10.1088/2041-8205/762/2/L30](https://doi.org/10.1088/2041-8205/762/2/L30)